AIS-2 RADIOMETRY AND A COMPARISON OF METHODS FOR THE RECOVERY OF GROUND REFLECTANCE

James E. Conel, Robert O. Green, Gregg Vane, Carol J. Bruegge, and Ronald E. Alley, Jet Propulsion Laboratory, California Institute of Technology, USA; Brian J. Curtiss, University of Colorado, Boulder, USA.

ABSTRACT

A field experiment and its results involving AIS-2 data for Rogers Lake, CA are described. The radiometry and spectral calibration of the instrument are critically examined in light of laboratory and ·field measurements. Three methods of compensating for the atmosphere in the search for ground reflectance are compared. We find, preliminarily, that the laboratory-determined responsivities are 30 to 50% less than expected for conditions of the flight for both short- and long-wavelength observations. The spectral sampling interval is 20 to 30 nm. The combined system-atmosphere-surface signal-to-noise ratio, as indexed by the mean response divided by the standard deviation for selected areas, lies between 40 and 110, depending upon how scene averages are taken, and is 30% less for flight conditions than for the laboratory. Atmospheric and surface variations may contribute to this difference. It is not possible to isolate instrument performance from the present data. As for methods of data reduction, the so-called scene average or log-residual method fails to recover any feature present in the surface reflectance, probably because of the extreme homogeneity of the scene. The empirical line method returns predicted surface reflectances that are systematically high but within a few percent of actual observed values using either calibrated or uncalibrated data. LOWTRAN-6, acting as an approximate theoretical model of the atmosphere for these exercises, predicts reflectance values 30 to 50% below the measured ones, based on the lower than expected radiances under solar illumination given by the instrument. This emphasizes the importance of accurate radiometric calibration in the study of surface or atmospheric properties.

INTRODUCTION

On October 14, 1986 the second version of the Airborne Imaging Spectrometer (AIS-2) with a 64- x 64-element HgCdTe array detector was flown over Rogers Lake, CA (Edwards Air Force Base) to (1) develop in-flight radiometric and spectral calibrations for the instrument and (2) compare the following three methods of compensation for the atmosphere in the recovery of ground reflectance: a scene-averaging (log-residual) technique, an empirical calibration line method, and a radiative transfer model. To support the radiative transfer modeling (the results of which are presented elsewhere [Conel, et al., 1987a]), ground measurements were made of atmospheric optical depth, the ratio of diffuse to direct incident light at the surface, and total precipitable water (cm^{-2}). Bidirectional spectral reflectance measurements of a bright lake bed and dark asphalt runway were made with a Portable Instant Display and Analysis Spectrometer (PIDAS) to

define empirical calibration lines of surface reflectance versus AIS response for the scenes generated during the overflight. Field spectral reflectance measurements of a concrete tarmac at North Base were taken as an unknown target against which results for the various methods of atmospheric compensation could be compared.

The primary focus of this paper is to describe the reduction of the AIS data to spectral radiance utilizing the detector responsivity equations developed by a laboratory calibration of the instrument with a $BaSO_4$-coated integrating sphere. From these data and from the spectral response to the standard ground targets, we develop estimates of the signal-to-noise ratio for laboratory and flight conditions. The effective in-flight instrumental spectral sampling interval is estimated by using atmospheric CO_2 absorption lines generated from LOWTRAN simulations. Some preliminary analyses of the atmospheric compensation problem are also described.

The AIS-2 instrument is described by Vane (1986). Discussed in this paper are observations made over two separate spectral intervals, 809-2143 nm and 1184-2523 nm, colloquially referred to as "tree" and "rock" mode observations, respectively.

FIELD MEASUREMENTS

Site Description and Flight Data

Rogers Lake (Lat. 34°55'N; Long. 117°50'W) is a dry playa located in Kern County, CA at an approximate elevation of 2270 feet (692 m) and contained within the Air Force Flight Test Center of Edwards Air Force Base. The flat, largely uniformly bright playa surface (Figure 1) is crossed by dark asphalt runways and is surrounded by terrain of low relief consisting of isolated rocky knobs and alluvial fans. The adjacent alluvial surfaces are covered with sparse desert scrub vegetation.

During the fall 1986 experiment, we acquired two lines of imaging spectral data, one in the rock mode (1184-2523 nm) and the other in the tree mode (809-2142 nm) at a flight altitude of 24,000 feet along roughly north to south tracks over the playa with vegetated terrain to the north.

Reflectance of Standard and Unknown Targets

Simultaneous with the overflight of AIS-2, spectral reflectance field observations were taken of three target areas within the AIS-2 field of view (Figure 1) using PIDAS. PIDAS has a spectral sampling interval of approximately 1 nm from 400 to 800 nm and 4 nm from 800 to 2500 nm (Goetz, 1987). The field spectra given in Figure 2 are averages from 30 to 60 sites. The field reflectance standard is $BaSO_4$. The targets are a uniformly high-reflectance playa surface and the low- and intermediate-reflectance runways. The runways of intermediate reflectance are used as an unknown in some of the atmospheric compensation studies described below. The standard deviation of all observations is everywhere less than a few percent and is greatest at longer wavelengths of observation, beyond about 2100 nm. Field observations were possible across the 1400-nm water
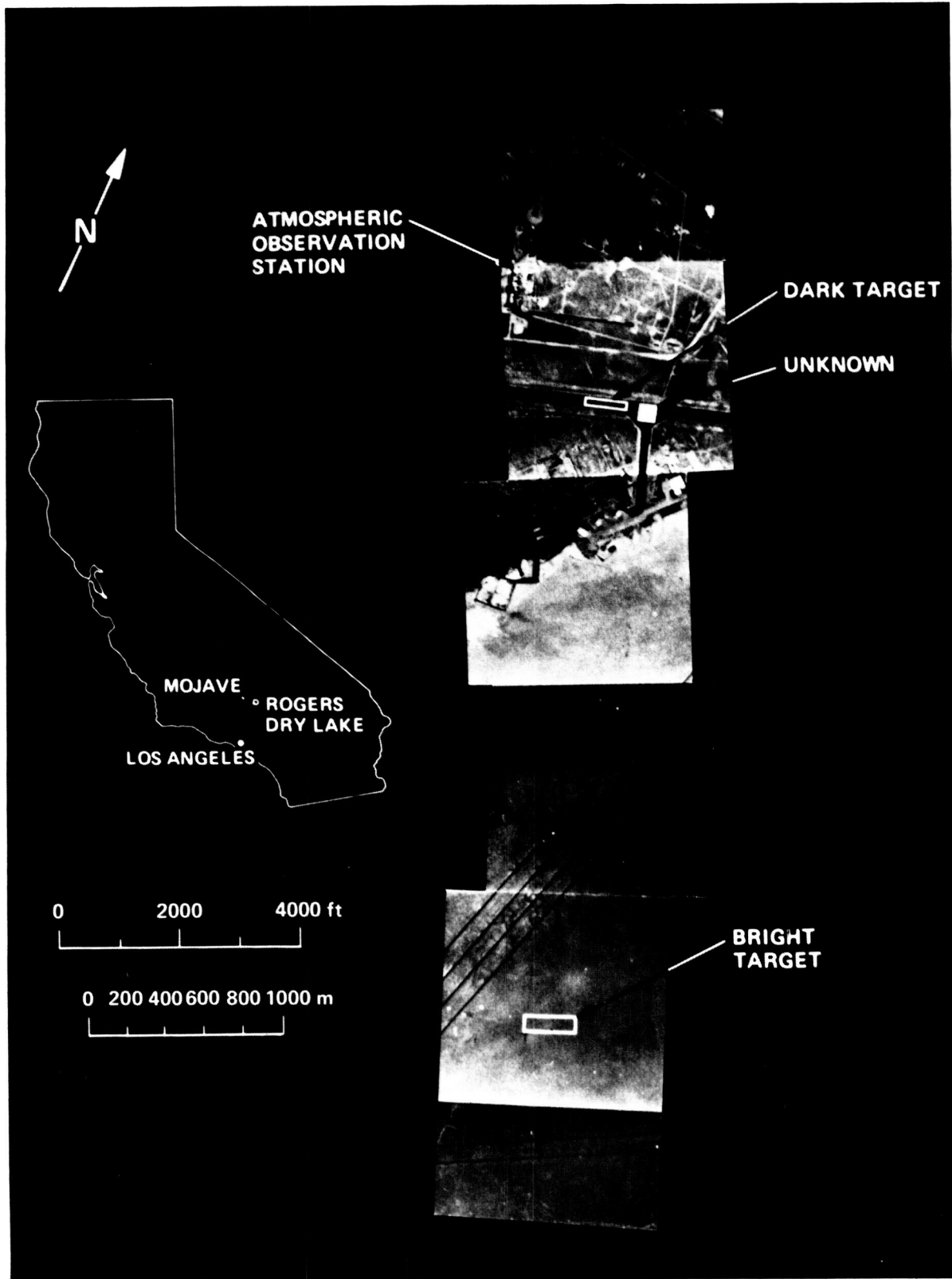
Figure 1. Locations of the October 14, 1986 AIS-2 calibration experiment at Rogers Lake, California
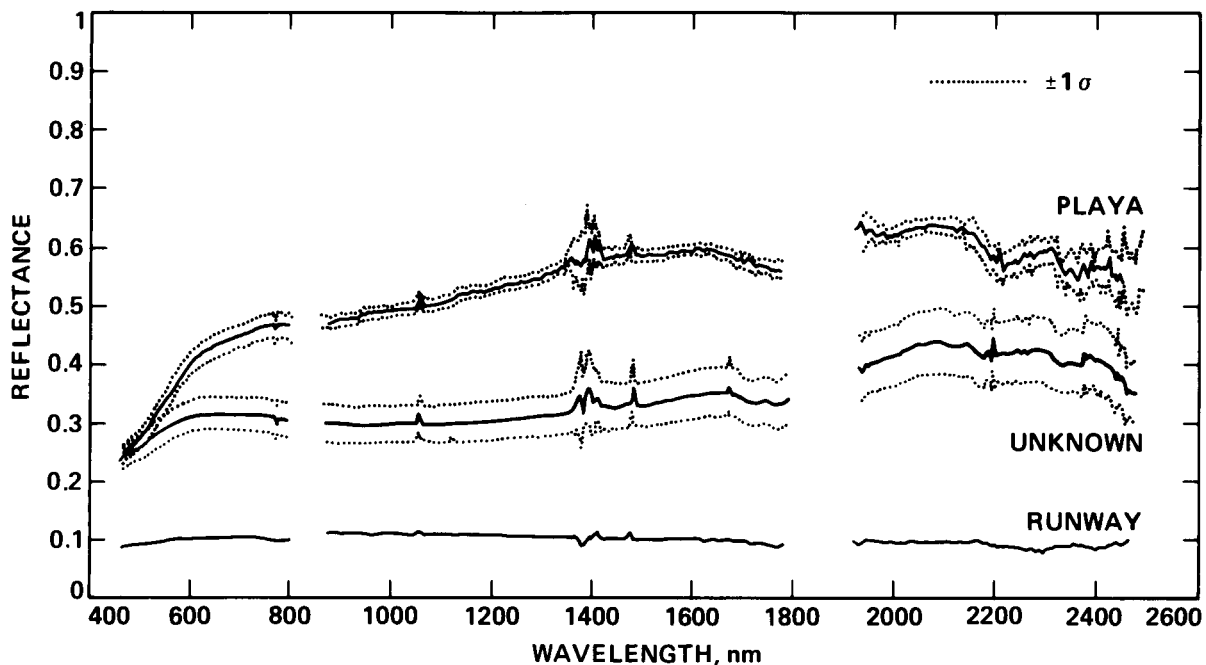
Figure 2. Spectral bidirectional reflectance of the standard and unknown targets as determined with PIDAS with respect to $BaSO_4$. Curves are averages ($\pm$ 1σ where shown) of 60 spectra for the playa and runway and of 30 spectra for the unknown target.

absorption feature, but the reflectance data have been deleted between 1800 and 1900 nm because of strong atmospheric interference. In addition, simple linear interpolations have been used to fill in gaps in these curves between 800 and 900 nm arising at the transition between spectrometers.

Measurements of Optical Depth

Measurements of incident solar illumination in the Thematic Mapper (TM) bandpasses were made with a standard Eppley Laboratories normal incidence pyrheliometer (NIPS) between 7:00 A.M. and 12:40 P.M. solar time on October 14. The data were cast in the form of conventional Langley plots of relative incident solar radiance versus air mass (1/cos [zenith angle]) and the optical depths for all filter bandpasses were determined from least square determinations of the slope. The results of these determinations are given in Table 1.

RADIOMETRIC CHARACTERISTICS FROM LABORATORY CALIBRATION

The purpose of the laboratory radiometric calibration of AIS-2 has been to establish the instrument's responsivity for each detector in each spectral sampling interval over a range of input radiances appropriate to the observation of natural targets. For the full 64 x 64 array, these calibrations lead·to the compilation of 8192 curves for both grating positions in each sampling mode.

Table 1. Optical Depths Determined in the TM Bandpasses
for the October 14 Experiment at Rogers Lake

Wavelength, nm	Optical Depth
485	0.195 ± 0.001
560	0.144 ± 0.001
660	0.080 ± 0.002
830	0.038 ± 0.001
1650	0.019 ± 0.002
2200	0.042 ± 0.003

The AIS-2 radiometric calibration employs a 40-inch integrating sphere coated with $BaSO_4$ whose spectral radiance is determined using an Optronics Laboratory Spectroradiometer. The spectroradiometer itself is calibrated against a standard illumination source that is National Bureau of Standards (NBS) traceable. The integrating sphere and spectroradiometer calibration procedures have recently been described by Tucker (1987). Aperture wheels placed between the externally mounted tungsten lamp sources and entrance ports of the integrating sphere control the radiance entering the sphere. The spectral radiance distribution of the integrating sphere measured as a function of channel and aperture wheel setting ([1], [2], ...) is shown in Figure 3 for the 1200- to 2500-nm spectral interval. The prominent absorption bands near channels 24 and 72 represent water present in the sphere coating. Some absorption from atmospheric path water may also be present. The major bands lie at somewhat shorter wavelengths, principally near channels 20 and 64, a difference that will serve to distinguish them from bands arising in the adsorbed or chemically bound component.

The response of AIS-2 to the assumed flat-field illumination, presented by the exit aperture of the integrating sphere and averaged over 500 lines of observations, is shown in Figure 4(a) for the greatest source illumination used in the calibration. The data are presented sequentially in terms of wavelength in blocks of 64, each block representing the spatial variation across a row. The beginning and ending detectors of each row (i.e., where each row represents 64 detector elements in one wavelength channel) show lower response than neighboring detectors. This is due to vignetting in the fore-optics. In addition to these strong edge effects, which may extend in a reduced amount further into the array, other periodicities as well as an overall gradient in response are apparent across each row. The origin of these various effects is, at this writing, unknown. The variation in mean detector response over all 128 bands is shown at a compact scale in Figure 4(b). The prominent water absorption features contributed by the integrating sphere appear near detector locations 1536 (channel 24) and 4600 (channel 72). A small discontinuity between grating positions is found at location 4096. The standard deviation of the set of 500 repetitive observations is not uniform with column number or channel. This variation is shown in Figure 4(c).
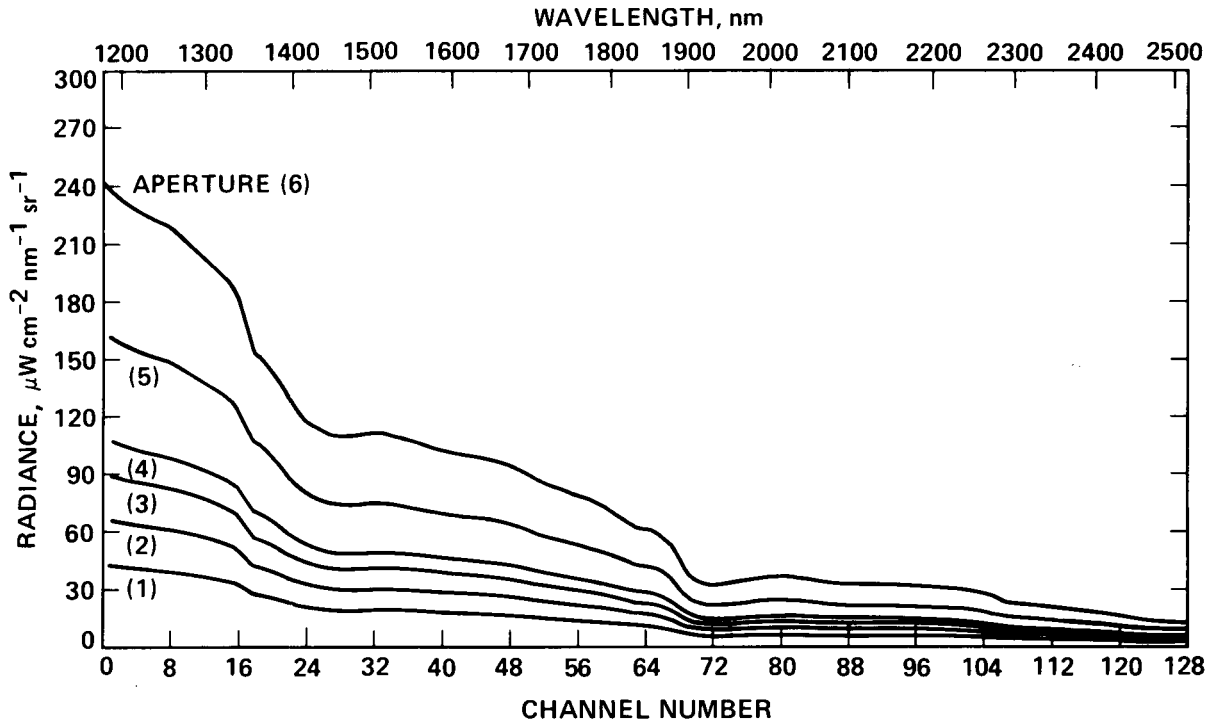
Figure 3. Spectral radiance of the integrating sphere (May, 1987) for the spectral interval 1185-2500 nm ("rock" spectral mode). Prominent absorption features near channels 24 and 72 are due to adsorbed or chemically bound water.

From the data of Figure 4(b), the response of any column of the detector array to illumination by the integrating sphere may be worked out. An example is shown in Figure 5 for column 3 (channel 3), with the spectrum corresponding to channel numbers 3, 67, 131, and so forth, of Figures 4(a) and (b). The major minima at channel numbers 24 and 72 again reflect water absorptions originating in the coating of the integrating sphere. An abrupt sawtooth variation occurs between grating positions. The finer jagged variations shown in Figure 5 are random variations in detector response, examples of which are depicted in Figures 4(a) and (b).

The responsivity equations represent relationships between the response of the imaging spectrometer and the input radiance. These relationships emerge by combining the plots of Figures 3 and 5 into a single diagram and by including the presence of an ND 0.9 filter in the optical train of AIS during its calibration. Examples are shown in Figure 6.

WAVELENGTH ASSIGNMENTS OF CHANNELS

To establish a correspondence between the channel number of the imaging spectrometer and the wavelength, we used the positions of atmospheric CO_2 and water vapor absorption lines of a model LOWTRAN-6 spectrum to fix in wavelength all identical, resolvable absorption bands in the AIS data. The wavelengths of 8 to 10 additional atmospheric bands from the LOWTRAN spectra

23
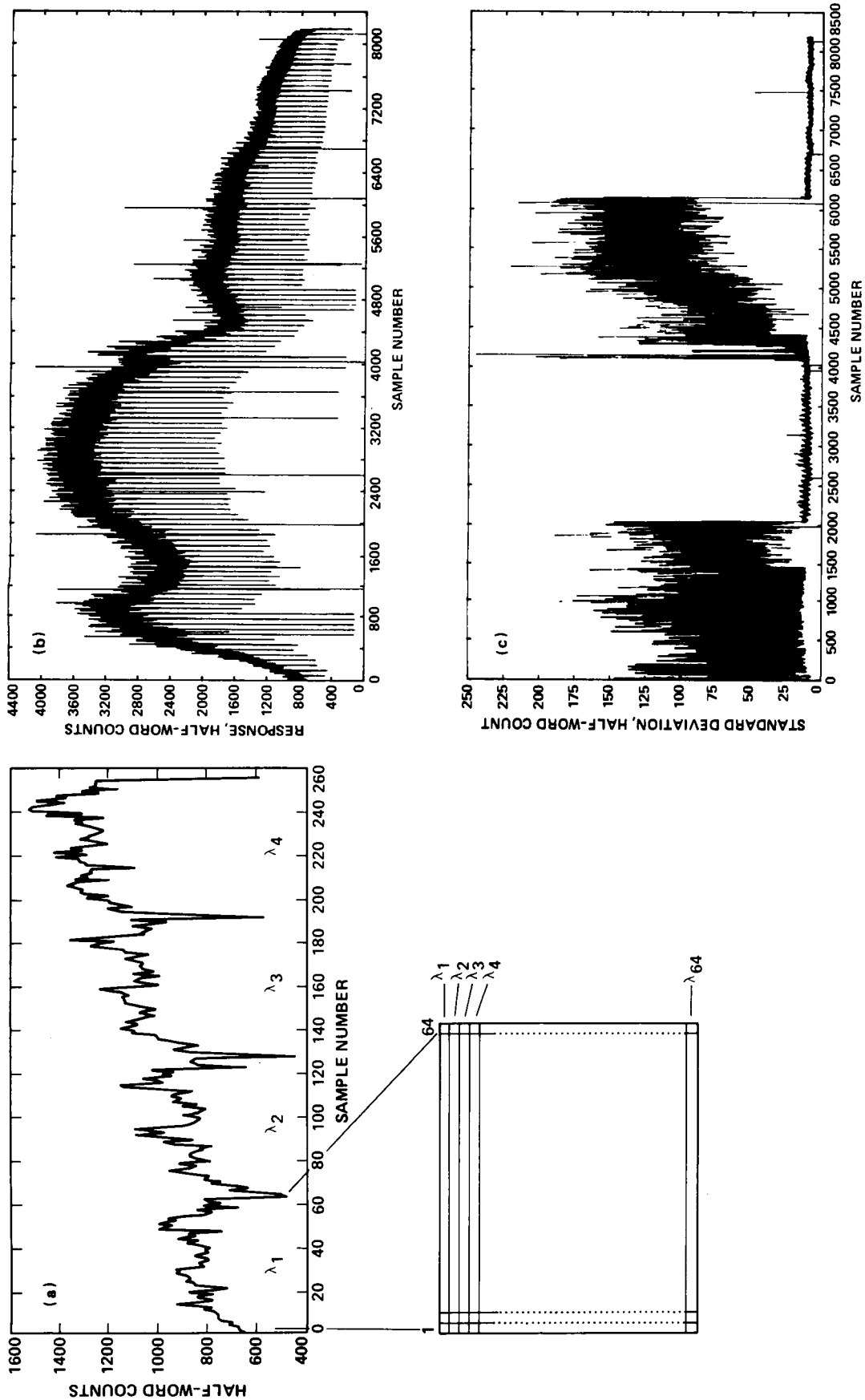
Figure 4. Mean spectral response of the AIS detector (64 x 64 HgCdTe) under flat-field illumination of the integrating sphere for an average of 500 lines: (a) Detailed variations for the first four wavelengths across rows of the array; (b) a compressed version of the spectra shown in 4(a) but covering channels 1-128 (1185-2522 nm); and (c) standard deviation of the 500 samples.

24
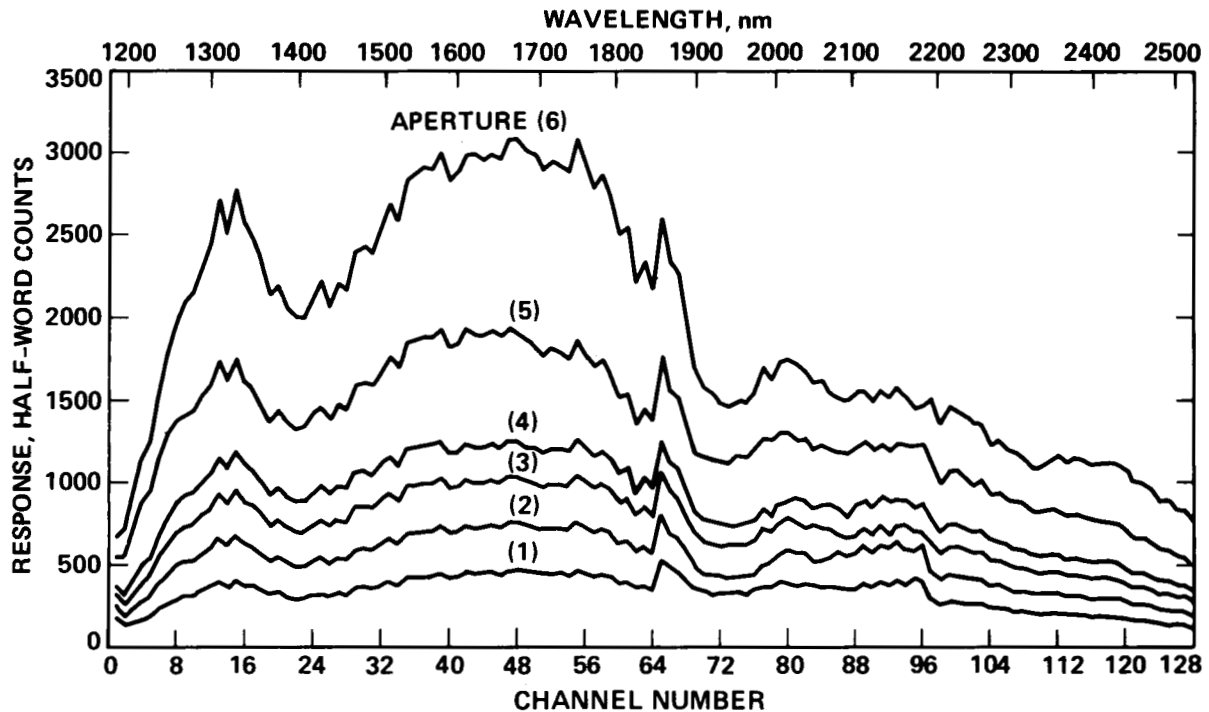
Figure 5. An example of detector response for the column 3 array, determined from the data of Figure 4. Note the discontinuity in responses between channels 64 and 65.

not detected in the observations were identified by channel numbers, and the complete sets of wavelengths and channel numbers were regressed against one another. The resulting equations relating wavelength to channel number N are

$$\lambda(nm) = 799 + 10.54 \ N$$

for $809 \leq \lambda \leq 2143$ nm with $r^2 = 1.0000$ and

$$\lambda(nm) = 1174 + 10.54 \ N$$

for $1184 \leq \lambda \leq 2523$ nm with $r^2 = 0.9999$. For both equations, $1 \leq N \leq 128$. The wavelengths provided from these equations for the beginning and ending of each measurement interval are in accord with positions measured with a standard monochromator in the laboratory to within 6 nm or better except for the long wavelength limit provided by the first equation above. The predicted wavelength is 2143 nm, and the measured is 2132 nm. Since this is very close to one channel, it seems probable that the single equation provided does not represent precisely the channel assignments for both grating positions, assuming the same slope requires an adjustment of the constant in the first equation to 788 nm for $65 \leq N \leq 128$. However, this adjustment has been ignored in practice (see below).
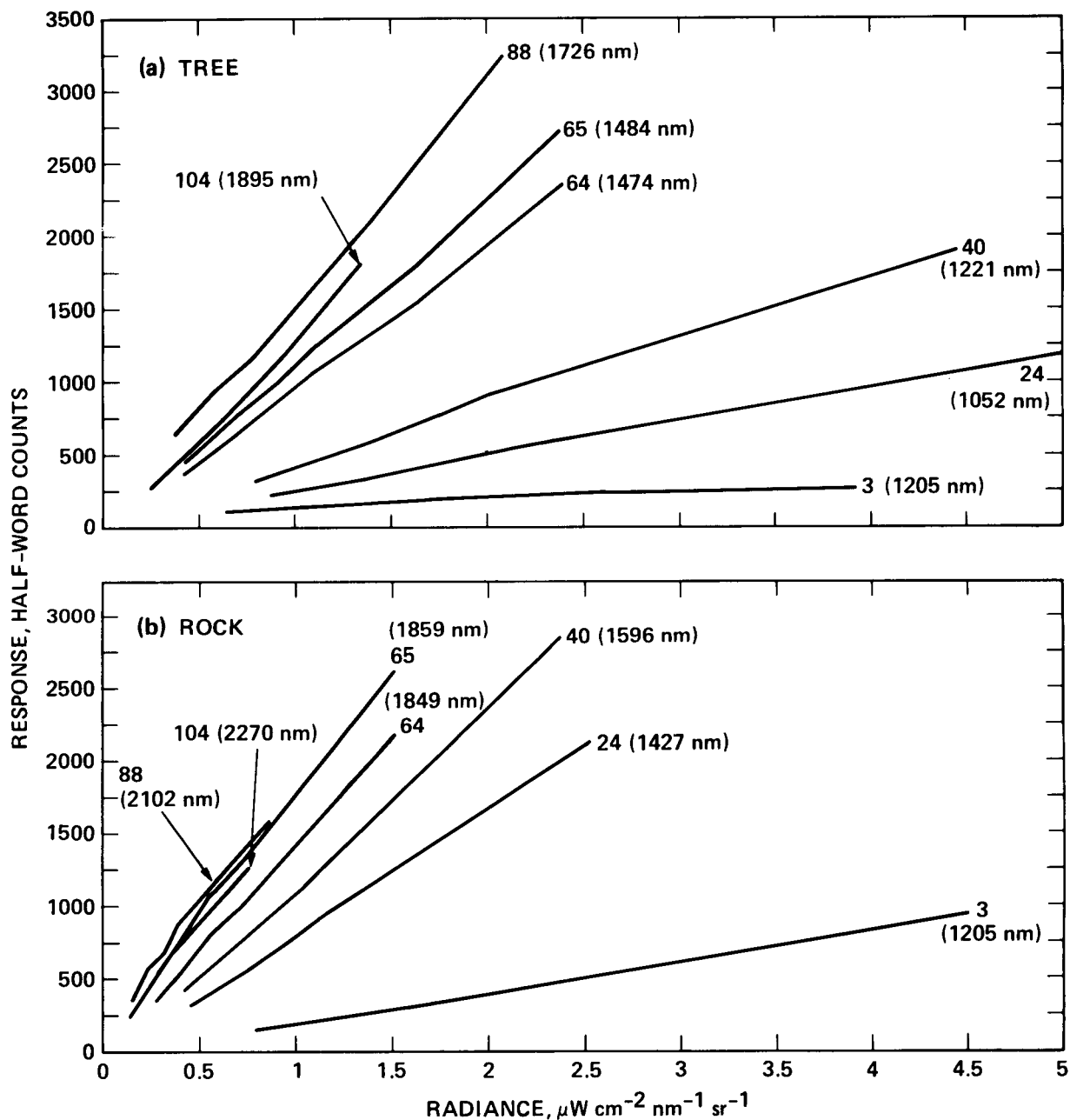
Figure 6. Response curves for detectors of column 3 in the array

ESTIMATION OF AN EFFECTIVE IN-FLIGHT SPECTRAL SAMPLING INTERVAL

Based on the wavelength calibration equations given in the previous section, the limiting spectral sampling interval is very close to 10.5 nm for both tree and rock mode observation intervals. To provide a measure of the in-flight effective sampling interval, we compared raw AIS spectra of the bright playa surface stated in terms of half-word DN with irradiance at the instrument as provided by LOWTRAN-6, and calculated at a spectral resolution of 10 cm^{-1} or about 2 nm. Apart from major absorptions related

to atmospheric water near 1400 and 1900 nm, the only additional bands of atmospheric origin resolved or unresolved in the AIS spectra arise from CO_2. We compare in Figure 7 the observed AIS playa spectrum with five LOWTRAN simulations, one at full resolution, and the others degraded using square filters of spectral width 20, 30, 40, and 100 nm. The prominent CO_2 absorptions near channel 40 (specifically 1572 and 1603 nm) are resolved at 20 but not at 30 nm, and thus the spectral sampling interval is probably between 20 and 30 nm. At a filter width of 40 nm the pair of CO_2 features near 2000 nm are just resolved, and any vestige of these is entirely removed at 100 nm. (These simple considerations may explain the highly variable but generally reduced or missing CO_2 absorptions and the smaller than anticipated and distorted water band absorption features in AIS-1 data, as reported by Conel et al. [1987b] and as resulting from a significantly degraded spectral sampling interval in those data, on the order of 50 nm or perhaps greater.)

On the expectation that the apparent signal-to-noise ratio could be improved by averaging large numbers of pixels, thereby suppressing the noise component of any spectral degradation present, we produced AIS spectra composed of averages of 1, 25, and 100 pixels over the playa. No improvement in the effective separation of either the 1600-nm or the 2000-nm set of CO_2 bands was achieved by these averaging procedures.
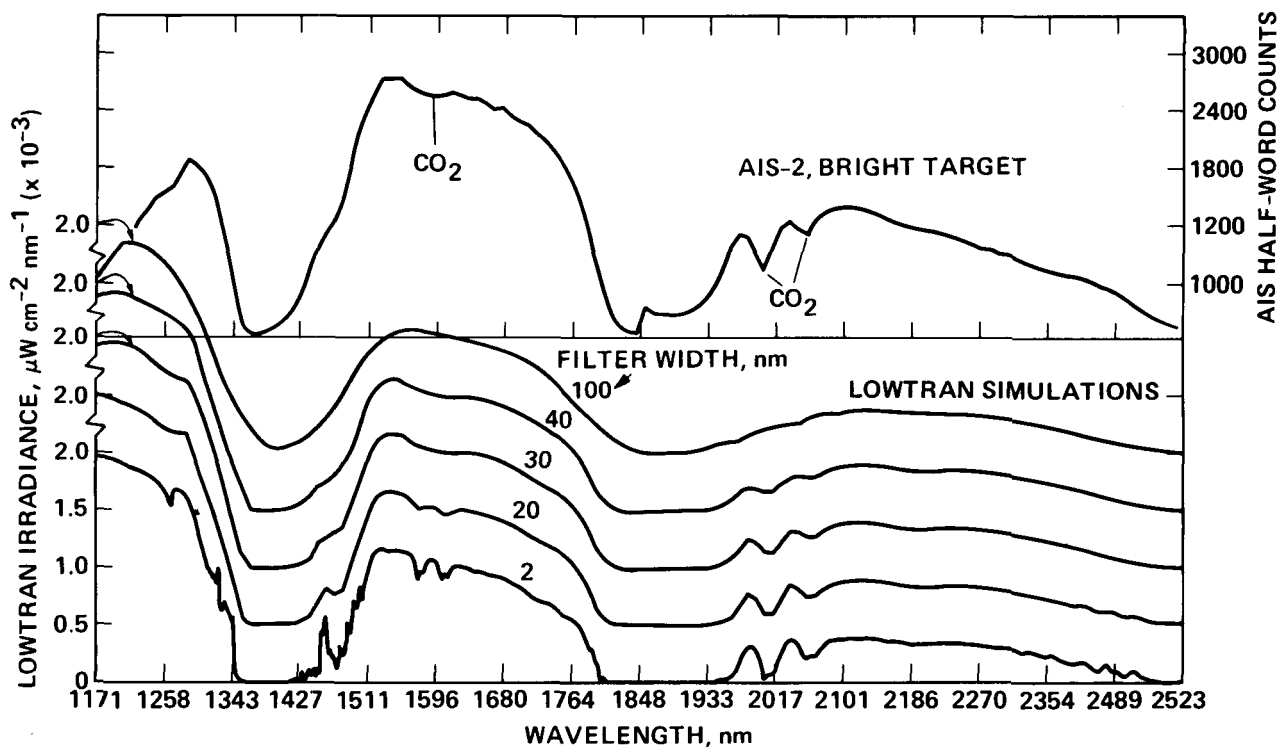
Figure 7. Examples of degradation of LOWTRAN spectra with square filters and comparison with observed AIS-2 spectrum for a target simulating a bright playa surface. AIS-2 has an equivalent spectral sampling interval between 20 and 30 nm.

27

REDUCTION OF FLIGHT DATA TO RADIANCE AND COMPARISONS WITH EXPECTED SOLAR RADIANCE AT THE INSTRUMENT

An important test of the validity of the laboratory determined responsivities (e.g., the curves of Figure 6) for flight conditions, and in addition the data reduction procedures, is the calculation of radiance at the instrument for a ground target of known reflectance. These results can be compared with radiances expected for a detailed atmospheric model. A simple method is to calculate the radiance expected at the instrument in a region of high atmospheric transparency (e.g., near 1200 or 1700 nm) and compare it to the radiance predicted from the responsivities at these wavelengths. The radiance $L(\lambda)$ is approximately equal to $\mu_0 F_0(\lambda) R(\lambda)$ where $\pi F_0(\lambda)$ is the seasonally adjusted solar irradiance at λ, μ_0 is the cosine of the solar zenith angle, and $R(\lambda)$ is the surface spectral reflectance. This procedure was followed by Conel et al. (1987a, 1987b) for the AIS-1 radiometric calibration study. The more elaborate calculation, taking into account atmospheric attenuation and scattering, involves computing the expected radiance at the aircraft from a realistic atmospheric model throughout the entire spectrum. This is the procedure adopted here, where for the sake of expediency we employ the standard midlatitude winter model of LOWTRAN-6 in the comparisons. However, the LOWTRAN model is only approximate, in particular accounting for only a single order of scattering at shorter wavelengths. The comparisons are therefore approximate although we scale results for the standard model at longer wavelengths ($>$ 830 nm) using our field-determined optical depths.

In Figure 8 we present the spectral radiance from the standard bright playa target expected according to (1) the LOWTRAN-6 simulation utilizing the field measured reflectance in Figure 2 and (2) AIS-2 utilizing the laboratory determined responsivities, examples of which have been given in Figure 6. Data from both instrument configurations (rock and tree modes) are shown. According to these determinations, the predicted AIS responses are lower than the LOWTRAN simulations by 30 to 50% for the longer wavelength data (rock mode) and by 30 to 40% for the short wavelength data (tree mode). To assess the appropriateness of the midlatitude winter model LOWTRAN simulation for this comparison, we give the optical depths measured on October 14 and the optical depths derived from the LOWTRAN atmospheric transmittances averaged over the TM bands in Figure 9. The LOWTRAN optical depths are larger at all wavelengths, but of particular significance are the differences at 1650 nm and 2215 nm because aerosol and Rayleigh scattering are negligible at these wavelengths and would not contribute significantly to the LOWTRAN-derived numbers no matter how scattering is accounted for in the LOWTRAN model. We estimate the adjustments required in the LOWTRAN-derived radiance curves from the relationship

$$L(\text{AIS conditions}) = L(\text{LOWTRAN conditions})$$

$$\times \ [T_{dn} \ (\text{AIS}) T_{up} \ (\text{AIS})/T_{dn}(\text{LOWTRAN}) \ T_{up}(\text{LOWTRAN})]$$

where $L(\text{AIS conditions})$ is the radiance for the optical depth appropriate to the AIS observing date, $L(\text{LOWTRAN conditions})$ is the radiance from the
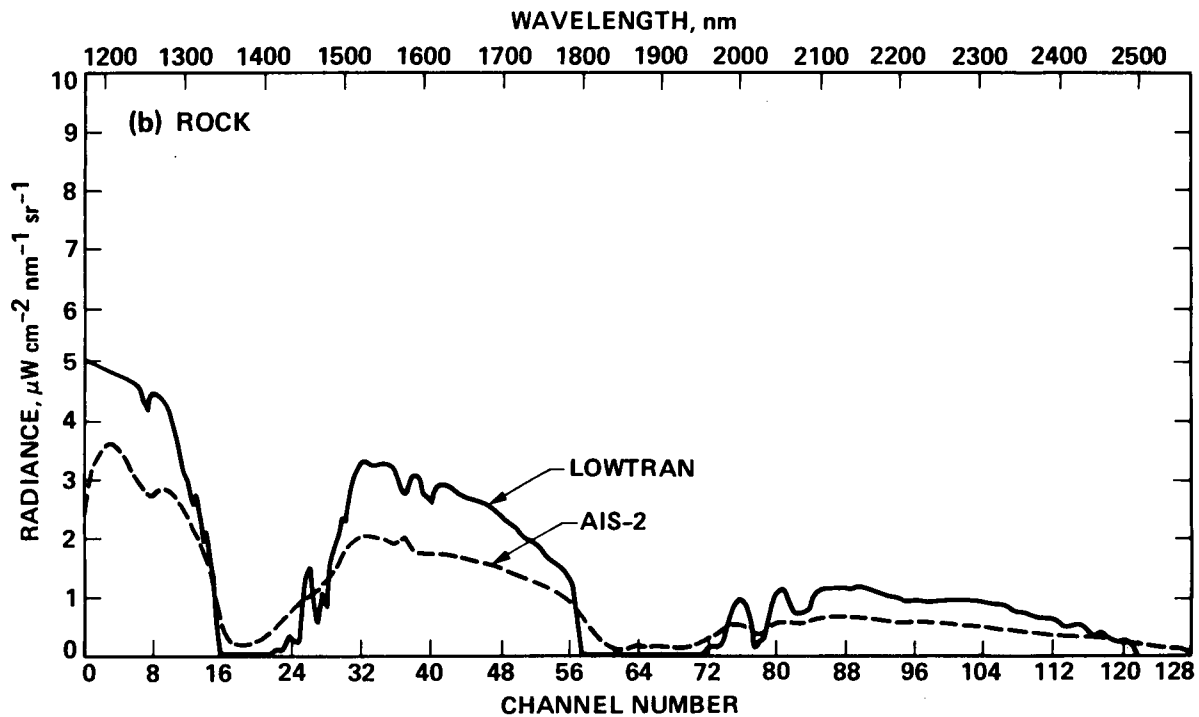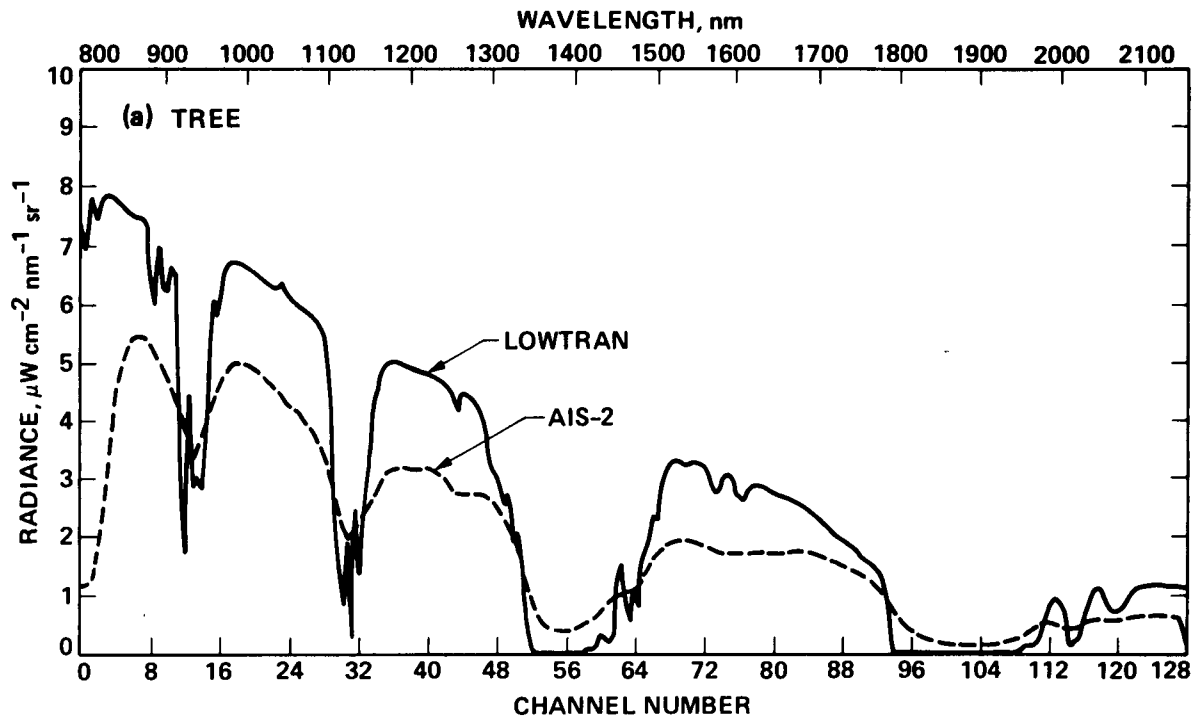
Figure 8. Examples of the reduction of raw AIS-2 half-word spectra to radiance compared to LOWTRAN simulations of the radiance expected at the instrument for the measured surface reflectance. The standard mid-latitude model for October 14, 1986 is used.
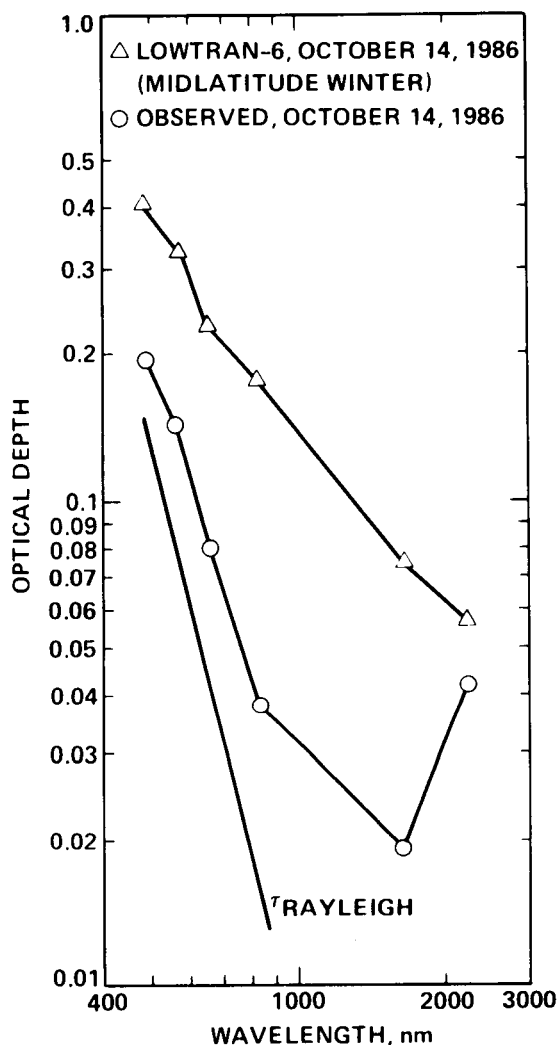
Figure 9. Comparison of optical depth measured for the site on October 14, 1986 with LOWTRAN optical depths at the same wavelengths. The optical depth for Rayleigh scattering, $\tau_{RAYLEIGH}$, is from a formula by Hansen and Travis (1974).

standard LOWTRAN model, and T_{dn} and T_{up} are the atmospheric trans-
mittance for the downward and upward paths, respectively. Specifically,

$$T_j = \exp[-\tau_j/\mu_j]$$

where j = either up or down, and μ_{dn} = cos (42.6 deg) for the downward
leg and μ_{up} = unity for the upward portion. For the two long-wavelength
TM bands the ratio L(AIS)/L(LOWTRAN) is given in Table 2. Note that T_{up}
(AIS) is calculated assuming the same proportional reduction in optical
depth between up and down paths as LOWTRAN. As expected, radiances
calculated from LOWTRAN relevant to the time of AIS observations need to be
increased; the discrepancies between the model and observations accordingly
widen somewhat.

SECOND ORDER MIXING AND STRAY LIGHT CONTAMINATION

The problem of spectral contamination from overlapping orders of
diffraction from the grating in AIS-1 data was discussed in detail by Conel

30

Table 2. The Ratio L(AIS conditions)/L(LOWTRAN conditions) for
TM Bands 5 (1650 nm) and 7 (2215 nm)

Band	T_{dn}		T_{up}		L(AIS)/
	AIS	LOWTRAN	AIS	LOWTRAN	L(LOWTRAN)
1650	0.974	0.903	0.996	0.986	1.091
2215	0.944	0.926	0.990	0.987	1.024

et al. (1986, 1987b), and by Cocks et al. (1986). This problem has been
eliminated in AIS-2 by the use of appropriate order sorting filters (see
Airborne Imaging Spectrometer Supplement, 1986) except at wavelengths longer
than 1600 nm in tree mode observations and beyond 2400 nm in rock mode. The
nature of this problem is illustrated in Figure 10, where both the long- and
short-wavelength radiometrically calibrated data for the standard bright
playa target are displayed together.

A residual radiance is also present within the 1400- and 1900-nm water
absorption bands for both rock and tree mode spectra and is somewhat greater
in the latter (Figure 8). Such residuals in bands thought to be saturated
are a concern from the standpoint of the possible presence of stray light.
During the time of overflight we also measured precipitable water with a
spectral hygrometer. This instrument handily indexes the water present by
looking at the sun and measuring the ratio of water band depth to continuum
height with two narrow filters (880 and 935 nm). These ratios are
calibrated against numerous radiosonde observations where the distribution
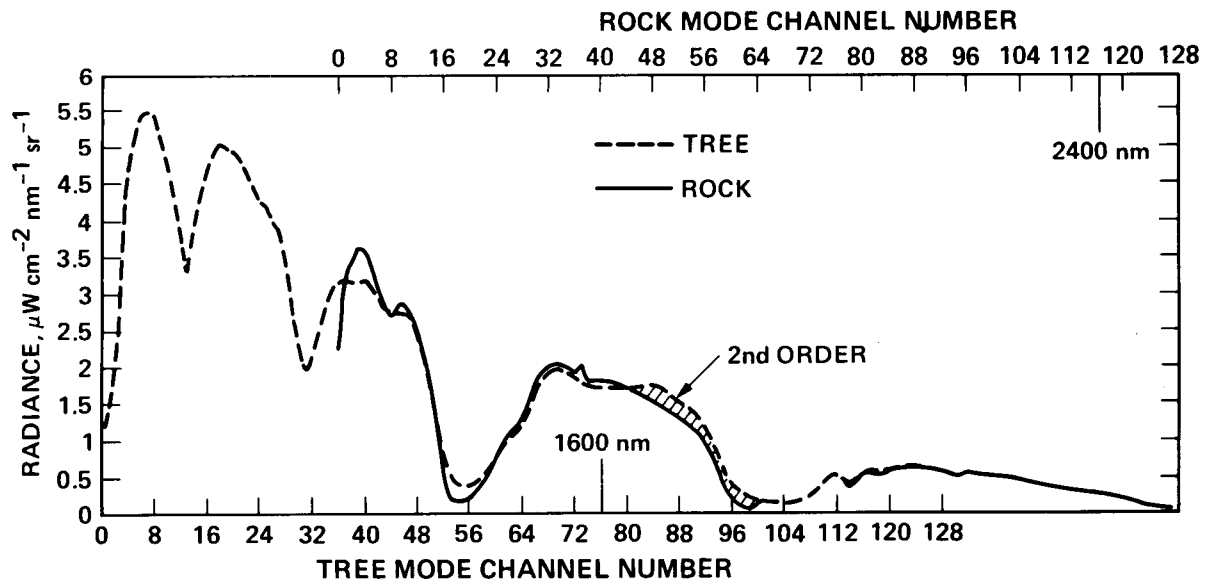
Figure 10. Comparison of rock and tree mode spectra to show the pos-
sible presence of a second order component

of water with height is measured (B. Gary, JPL, personal communication, 1986). Near 11:30 A.M. solar time, the vertical column abundance was determined to be 0.47 gm/cm^{-2}, which for a solar zenith angle of 42 deg gives about 1.1 gm/cm^{-2} for the total water present in the path. This value is slightly less than that assumed in the standard LOWTRAN-6 model (about 0.6 gm/cm^{-2} total in the vertical column or 1.41 gm/cm^{-2} over the path). The expected atmospheric transmittance was estimated for the measured water abundance using the formula and absorption coefficients given by LaRocca (1978, Eq. 5.53 and Table 5-4). At 1400 nm the transmittance was calculated to be 3%, whereas the measured value is close to 12%; at 1900 nm the transmittance is 2%, and the measured value roughly 15%. These approximate determinations suggest the possible presence of stray light in the instrument.

REMOVAL OF UNEQUAL DETECTOR RESPONSE IN IMAGERY

Once the laboratory-determined responsivities (or instrumental light transfer curves) are available, it is not difficult to reduce the raw image data to radiance, thereby eliminating the effects of variable detector response. The effect of this transformation on the image data is illustrated in Figure 11 for channels 48 through 64, where a considerable reduction in vertical striping with calibration and a consequent enhancement in surface detail can be seen.

ESTIMATION OF SIGNAL-TO-NOISE RATIO

The playa surface presents a large, uniform target with a spectrum that varies more or less slowly with wavelength. We attempted to take advantage of these features to make estimates of the system signal-to-noise ratio using the radiometrically corrected imaging spectrometer data. The radiometrically adjusted data can be expected to yield somewhat better values than the raw spectra because the random variations in detector responsivity, examples of which are shown in Figure 4(a), have been reduced. This is evident by comparing the radiometrically calibrated and uncalibrated images in Figure 11. We take as estimates of the signal the mean value of the radiance averaged over row, column, or area, all for a single wavelength. The noise estimate is provided by the standard deviation of the observations. The mean (μ), standard deviation (σ), and the ratio (μ/σ) are plotted in Figure 12 for various cases involving row, column, and areal averages, all beginning in column 17 of the detector array and for Channel 40 (1592 nm). Figure 12(a) gives the laboratory result derived from flat-field illumination with the integrating sphere and isolates the variation in the quantities plotted for a single detector. For this artificial illumination the value of μ/σ is about 180. A similar average for flight conditions is shown in Figure 12(b). The estimated signal-to-noise ratio is seen to be reduced about 30% for flight conditions, but the significance of this apparent reduction needs discussion.

In addition to a possible reduction in performance of the system under flight conditions, there are sources of variation inherent in the standard target over the area sampled and variations in the atmospheric conditions
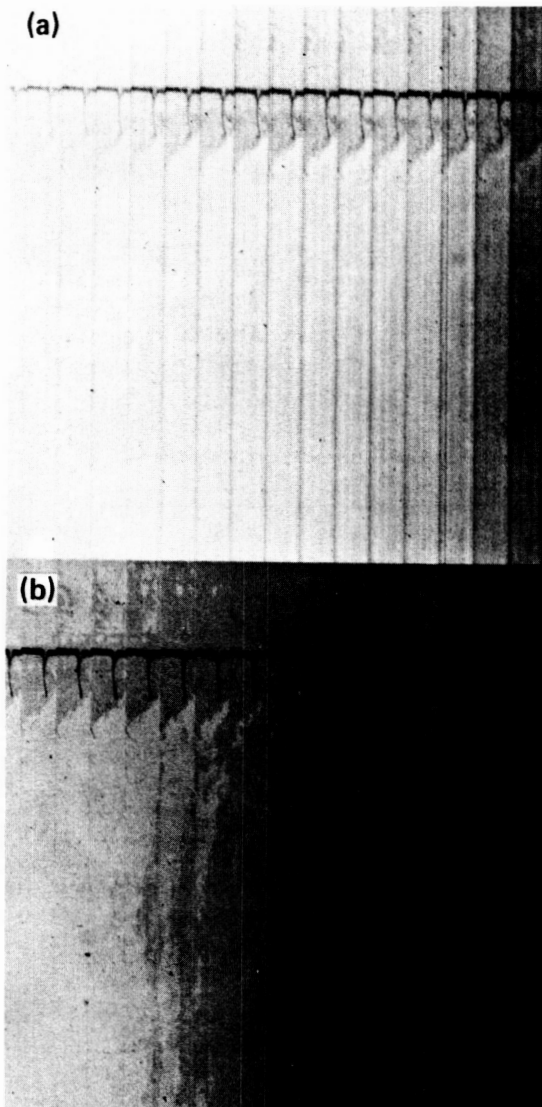
Figure 11. Removal of vertical striping with accompanying radiometric calibration of AIS-2 data: (a) before calibration and (b) after calibration.

over paths from the instrument to these samples. Let us consider the propagation of uncertainties from such sources. (We assume a nonscattering atmospheric model of two-way transmittance T and a linear instrument responsivity with gain factor G connecting the output [in DN] and radiance at the instrument [L]. The model will be described in more detail below.) A straightforward calculation leads to the formula for the fractional standard deviation (squared) of the DN

$$(\sigma_{DN}/DN)^2 = (\sigma_R/R)^2 + (\sigma_T/T)^2 + (\sigma_G/G)^2$$

Here, σ_{DN}^2, σ_R^2, σ_T^2 and σ_G^2 are the variances of, respectively, the DN, surface reflectance, atmospheric transmittance, and instrumental gain factor. We have assumed that instrumental noise sources can be represented as random variations in the gain factor alone. This equation gives an estimate of σ_G/G under flight conditions when the other terms are

33
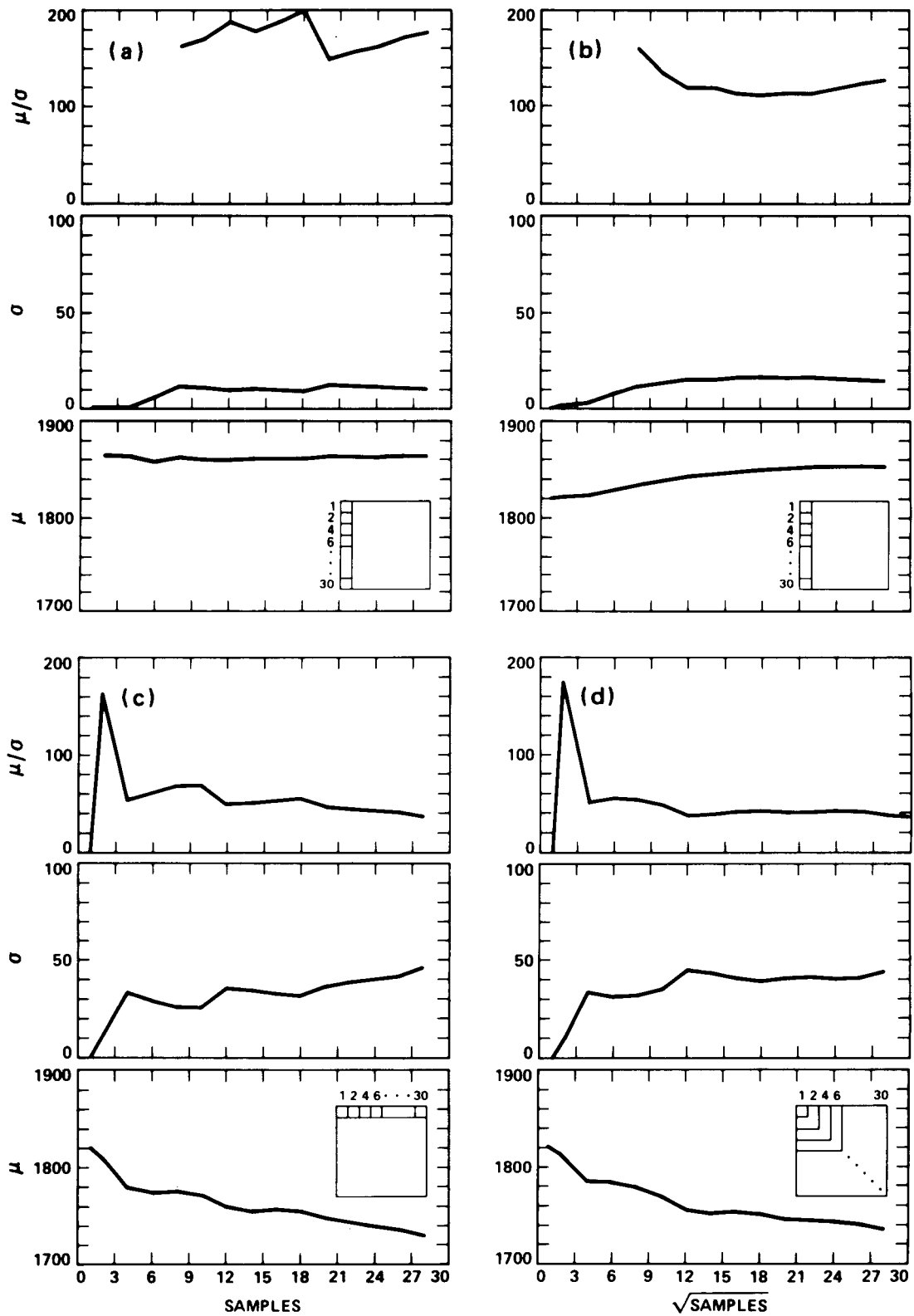
Figure 12. Variation of mean (μ), standard deviation (σ), and ratio for pixel samples of various sizes and configurations on the playa.

determined. A numerical value for the left-hand side is obtained from the flight data for the standard target, given in Figure 12(b). This value is about $(1/110)^2$. From Figure 2, at 1592 nm, the first term on the right-hand side measuring the fractional variance of R is about $(1/60)^2$. Adopting this number assumes the PIDAS measurements themselves are error-free. This is certainly questionable considering that the determination of the ground reflectance itself depends upon two observations (target and reference) that individually are functions of all the factors described in the model above plus possible operator variability stemming from the fact that the instrument is hand-held. (One of us [R.O.G.] has made a preliminary study of the repeatability of PIDAS measurements. For 20 consecutive observations of a target and reference spanning a period of a few minutes, the scatter in the calculated reflectance is about one part in thirty.) With respect to fluctuations in T, no direct measurements are available of atmospheric variability over the paths and on a time scale commensurate with the frequency of data acquisition (16 lines/sec). We used our measurements of diffuse and direct incident total radiation acquired during the experiment to establish approximately the magnitude of the variability over periods on the order of a few minutes. From the analog records, the ratio of peak to peak variability of the diffuse light to the total of diffuse and direct components is 1/1700. No variation in the direct component itself can be detected from the record. These observations suggest that for the present calculations, the sky variation is negligible.

Comparing the magnitudes of the various terms just given shows the fractional variance of the surface reflectance to be by far the largest term, which is inconsistent with the measured total value. Two possible causes of this problem may be (1) unrepresentative sampling of the surface at a pixel scale with PIDAS or (2) poor repeatability of the PIDAS observations themselves. Both of these questions will be the focus of future studies.

An alternative viewpoint is to adopt the laboratory determined fractional variance of G (i.e., σ_G/G is given by $1/(\mu/\sigma)$ in Figure 12(a), which is about $(1/180)^2$ and to ascribe the degeneration of the total fractional variance to the sum of uncertainties from atmospheric and surface sources. The combination of these two terms has a value of $(1/110)^2 - (1/180)^2$ or approximately $(1/140)^2$. It is certainly plausible that the differences observed between laboratory and flight values could be contributed by these sources that are totally dominated by variations in the target reflectance. Isolating instrument performance has remained elusive.

The variations observed in averages across columns, Figure 12(c) and, with area, Figure 12(d), are larger than those found in the row averages, and in general lead to the lower values of μ/σ of about 40. The across-column averages are thought to contain additional sources of banding in addition to that arising from variations in detector response already compensated for. This contributes to the larger scatter, and consequently lower signal-to-noise ratio, estimate.

REDUCTION OF THE RADIANCE DATA TO GROUND REFLECTANCE

In this section we compare the results of three largely independent methods that may be used to compensate for atmospheric effects in imaging spectrometer data: (1) scene average or residual, (2) empirical line, and (3) radiative transfer modeling. Similar studies comparing methods (1) and (2) were carried out by Roberts, et al. (1986). In principle, method (1) can be employed independent of any ground measurement wherever the atmosphere is uniform and the path radiance is zero. Methods (2) and (3) possess the same theoretical basis. In both, the scanner response (or radiance) can be arranged as an essentially linear function of ground reflectance. The fundamental difference in these two approaches from our point of view is that in the empirical method (2), the slope and intercept of the response curves at each wavelength are fixed by two-point ground observations of the reflectance, whereas in the modeling approach (3), these constants are calculated from theory after measurements of the optical depth and single scattering albedo have been used. In what follows, the parameter of interest is assumed to be surface spectral reflectance, although in other applications the atmospheric properties themselves might be of equal concern.

The strategy employed made predictions of the surface reflectance (by the methods mentioned) which were then compared with field-measured values. For this purpose, the unknown target of reflectance, whose spectrum is given in Figure 2, was used. Actually, for methods (1) and (3) this target as well as the two standard targets could have been used, while for method (2) only one target was available because two standards are used to construct the prediction relationships.

Residual or Scene-Averaged Method

An intriguing method of atmospheric compensation that is based entirely upon manipulation of the image data themselves without intervention of ground measurements is the residual (log-residual if logarithmic variables are employed) or scene average method (Green and Craig, 1985; Solomon, 1984). The radiance observed by an aircraft-mounted scanner system can be expressed as

$$L(x,y,\tau - \tau') = P(x,y,\tau - \tau') + T(x,y, \tau - \tau') R(x,y) \qquad (1)$$

where the coordinates of a particular point in the image are (x,y) and where τ and τ' refer to the total optical depth of the atmosphere and the optical depth of observation measured from the top downward. This notation suppresses the dependence of the quantities L, P, T, and R on wavelength, and directions of solar incidence and observation. The first term in Eq. (1) is path radiance and represents sunlight that is directly and diffusely transmitted by the upper part of the atmosphere (above the depth of observation) and that is reflected upward by the lower part of the atmosphere (below the depth of observation). The second term is directly and diffusely transmitted upwelling surface radiation. The surface reflectance, $R(x,y)$, is assumed to be Lambertian. It is further assumed that the scanner response has been converted to absolute radiance units for

all detector elements. The required steps are discussed elsewhere in this paper. For the long wavelength (rock) mode of observation (1180-2523 nm) the path radiance P is often negligible, so that Eq. (1) simplifies to

$$L(x,y,\tau - \tau') = T(x,y,\tau - \tau')\, R(x,y) \qquad (2)$$

For a homogeneous atmosphere, constant elevation of the terrain above sea level, and constant observation elevation and attitude of the aircraft, it would also be justified to assume $T(x,y,\tau - \tau') = \langle T(\tau - \tau')\rangle$, a constant independent of position. A simple method for estimating $\langle T(\tau - \tau')\rangle$ is to form averages of the radiance L (x,y) over the image area to get

$$\langle L\rangle = \langle T\rangle\, \langle R\rangle \qquad (3)$$

where $\langle L\rangle = (1/\text{Area}) \iint L(x,y)\, dxdy$, etc. Applying this to Eq. (2) particularized for constant transmittance $\langle T\rangle$ yields

$$L(x,y) = (\langle L\rangle/\langle R\rangle)R(x,y)$$

which expresses the scaled reflectances $R(x,y)/\langle R\rangle$ in terms of the image-derived quantities. If the atmosphere is inhomogeneous or the terrain uneven, or if the aircraft altitude above sea level and attitude are not constant, then averages of the image-derived radiances over the scene yield

$$\begin{aligned}
\langle L(\tau - \tau')\rangle &= (1/\text{Area}) \iint T(x,y,\tau - \tau')\, R(x,y)\, dxdy \\
&= T(u,v,\tau - \tau')\, \langle R\rangle \qquad (4)
\end{aligned}$$

where $T(u,v,\tau - \tau')$, by the mean value theorem, is some value contained in the set of $T(x,y,\tau - \tau')$ but is otherwise unconstrained. In this case, applying Eq. (4) to Eq. (2) yields

$$L(x,y)/\langle L\rangle = [T(x,y)/T(u,v)]\, [R(x,y)/\langle R\rangle] \qquad (5)$$

A key assumption required for the application of these methods is that the $\langle R\rangle$ produced by averaging is independent of wavelength. As emphasized by Solomon (1987, personal communication), this is never true for homogeneous scenes. For homogeneous terrain, $R(x,y)/\langle R\rangle \sim$ unity, and

$$L(x,y)/\langle L\rangle = T(x,y)/T(u,v) \qquad (6)$$

37

Thus the technique yields a function that is proportional to the transmittance properties of the atmosphere and that tends to be independent of the surface for the case of homogeneous ground reflectance.

In the following preliminary treatment we have used the raw half-word AIS data with the spectral analysis manager SPAM (SPAM Handbook, 1987). Using the uncalibrated numbers introduces additional factors related to detector responsivity into the analysis as follows. Assuming that dark current responses have been eliminated from the data, the relationship between radiance and instrumental response measured in DN is

$$L(x,y,\lambda) = DN(x,y,\lambda)/G(x,\lambda) \tag{7}$$

where $G(x,\lambda)$ is a gain factor that depends on column position in the detector array (x) and row position (λ) only. Assuming the atmospheric part to be homogeneous so that $T(x,y,\tau - \tau')$ is equal to a constant ($\langle T \rangle$, say), then approximately

$$\langle DN(\lambda) \rangle = \langle T \rangle G(u,\lambda) \langle R \rangle \tag{8}$$

where $G(u,\lambda)$ is some value of G found within the set $G(x,\lambda)$ but is otherwise not constrained. Thus,

$$DN(x,y,\lambda)/\langle DN(\lambda) \rangle = [G(x,\lambda)/G(u,\lambda)] \, [R(x,y,\lambda)/\langle R(\lambda) \rangle] \tag{9}$$

We studied the scaled surface reflectance function based on this formula for the unknown (runway tarmac) and bright (playa) targets for the rock mode observations. In Figure 13 these functions are compared to a LOWTRAN transmittance spectrum derived from the midlatitude winter model and to the surface bidirectional spectral reflectance for the site as measured at 2-nm spectral resolution with PIDAS. (Note: The assumption of zero path radiance, implicit in formulating equation [2], is probably not valid for the shorter wavelength portion of the tree mode observations, which extend in wavelength from 809 to 2143 nm.) For the most part, these spectra are dominated by the presence of atmospheric absorption bands, and it is difficult to isolate with confidence any feature of the surface spectrum in the log residual spectrum without the actual surface spectrum as a guide. These results may be explained by resorting to equation (6) and the discussion following that equation. The proposed similarity between $\langle R \rangle$ and $R(x,y)$ that may have generated this result will eventually be examined by a calculation of $\langle R \rangle$ from the empirical line method of recovering surface spectral reflectance, and will be compared with locally computed values via the same set of calibration relationships.

Empirical Line Method

The empirical calibration line method is very simple to apply in principle. Field observations are made of surface reflectance for
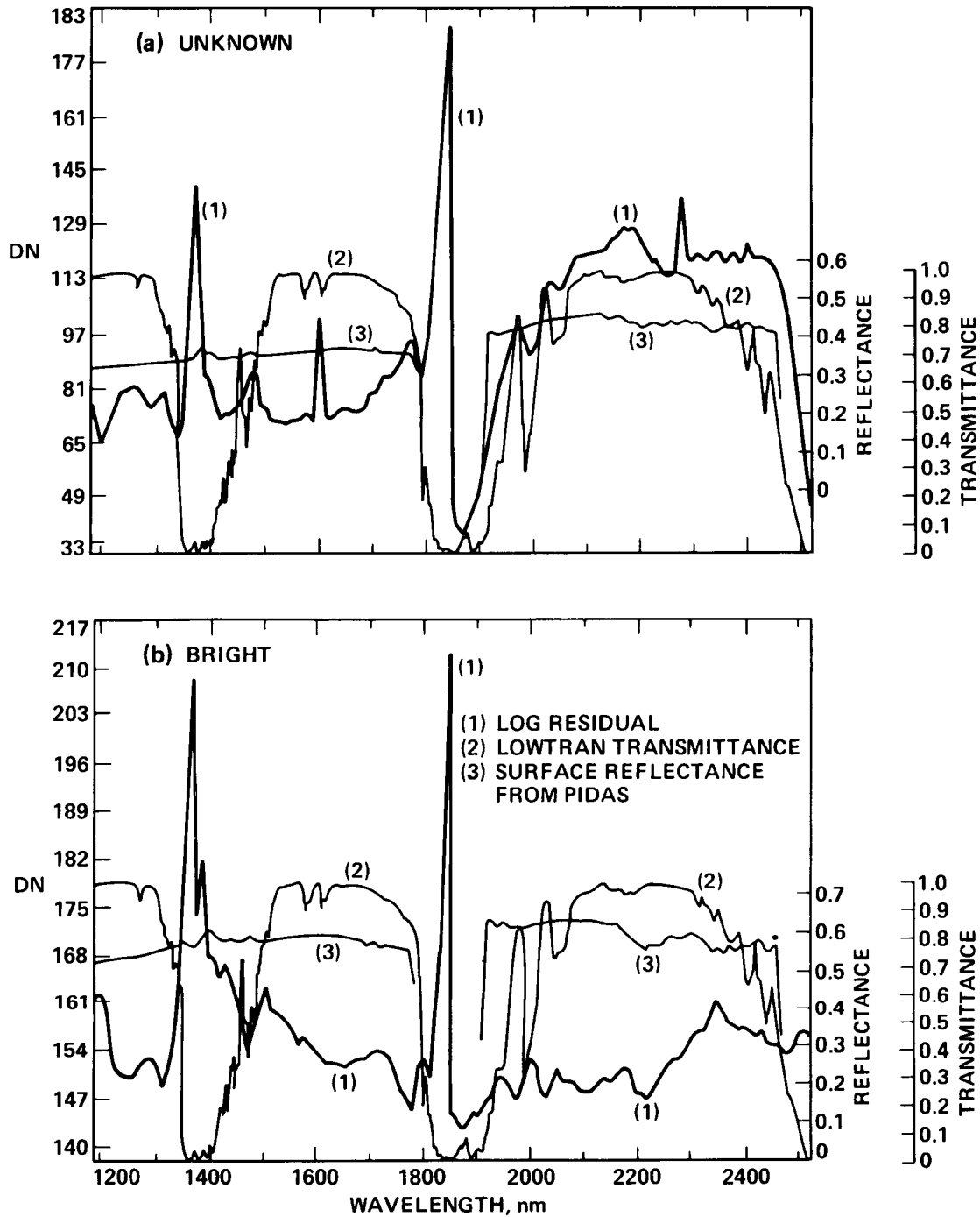
Figure 13. Comparison of spectra for two targets produced by the log-residual (scene average) method, a LOWTRAN transmission spectrum of the atmosphere, and the measured surface reflectance obtained from PIDAS.

homogeneous targets recognizable in the AIS imagery, and the scanner response for these areas is obtained. Plots of response (DN) (or radiance if the data are calibrated) vs surface reflectance are prepared as the basis

for compensation of the atmosphere elsewhere. Examples of two of the calibration lines obtained using the bright and dark targets are shown in Figure 14. The slope and intercept values L_0 and dL/dR in the relationship

$$L(k) = L_0(k) + [dL(k)/dR(k)] R(k), \quad k = 1, 2, \ldots, 128$$

are shown in Figure 15. The spectral variation of dL/dR is proportional to the two-way atmospheric transmittance as multiplied by the solar spectral radiance, which it functionally resembles, while L_0, which declines with wavelength, is the path radiance.

The empirical method is applied to the target with unknown reflectance, and the result compared to the field-observed spectrum in Figure 16. Both calibrated (radiance) and uncalibrated (half-word DN) data have been included in the transformations. The results of these two different reductions are comparable. On the whole the fit is good, but the predicted spectra are systematically greater in reflectance by a few percent than the observed spectra, except between about 2018 and 2280 nm where the departures reach about 5%. A small minimum in the predicted reflectances near 2017 nm straddles major atmospheric absorptions from CO_2, and may represent poor compensation for this species in the reductions.

The differences between observations and predictions by the present method must originate in the calibration lines themselves. Two potential sources of concern are (1) how well the field-measured reflectances represent the standard targets and (2) whether spatial resolution of the target of unknown reflectance in the imagery is good. With respect to (1),
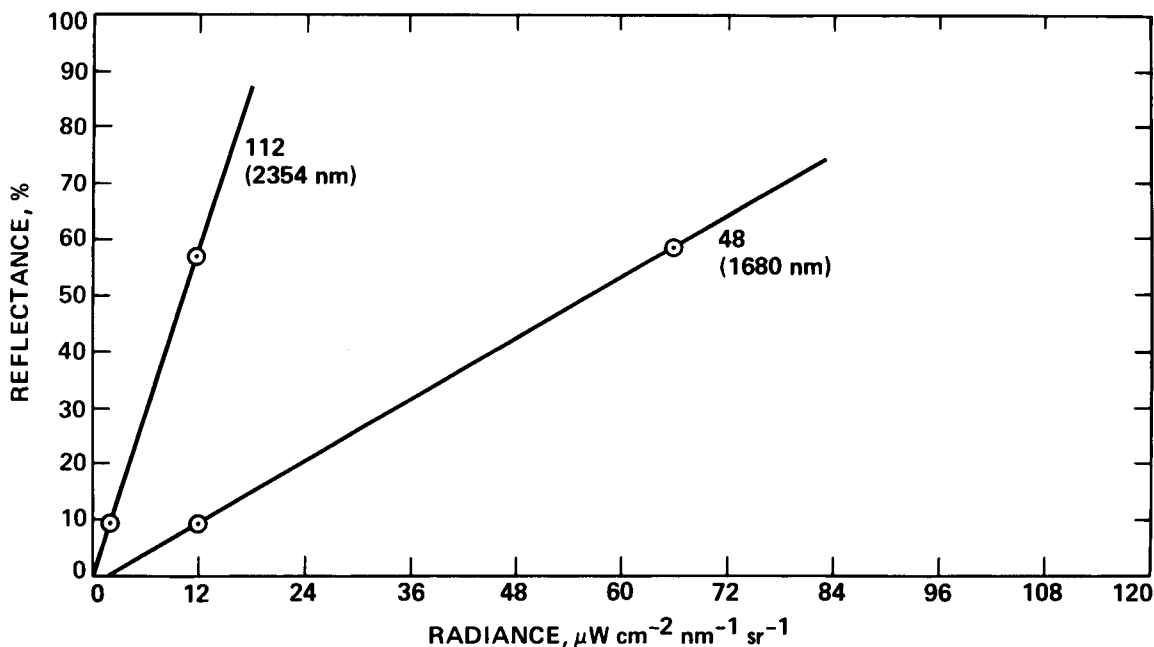
Figure 14. Examples of empirical calibration lines produced from bright playa and dark runway reflectance observations
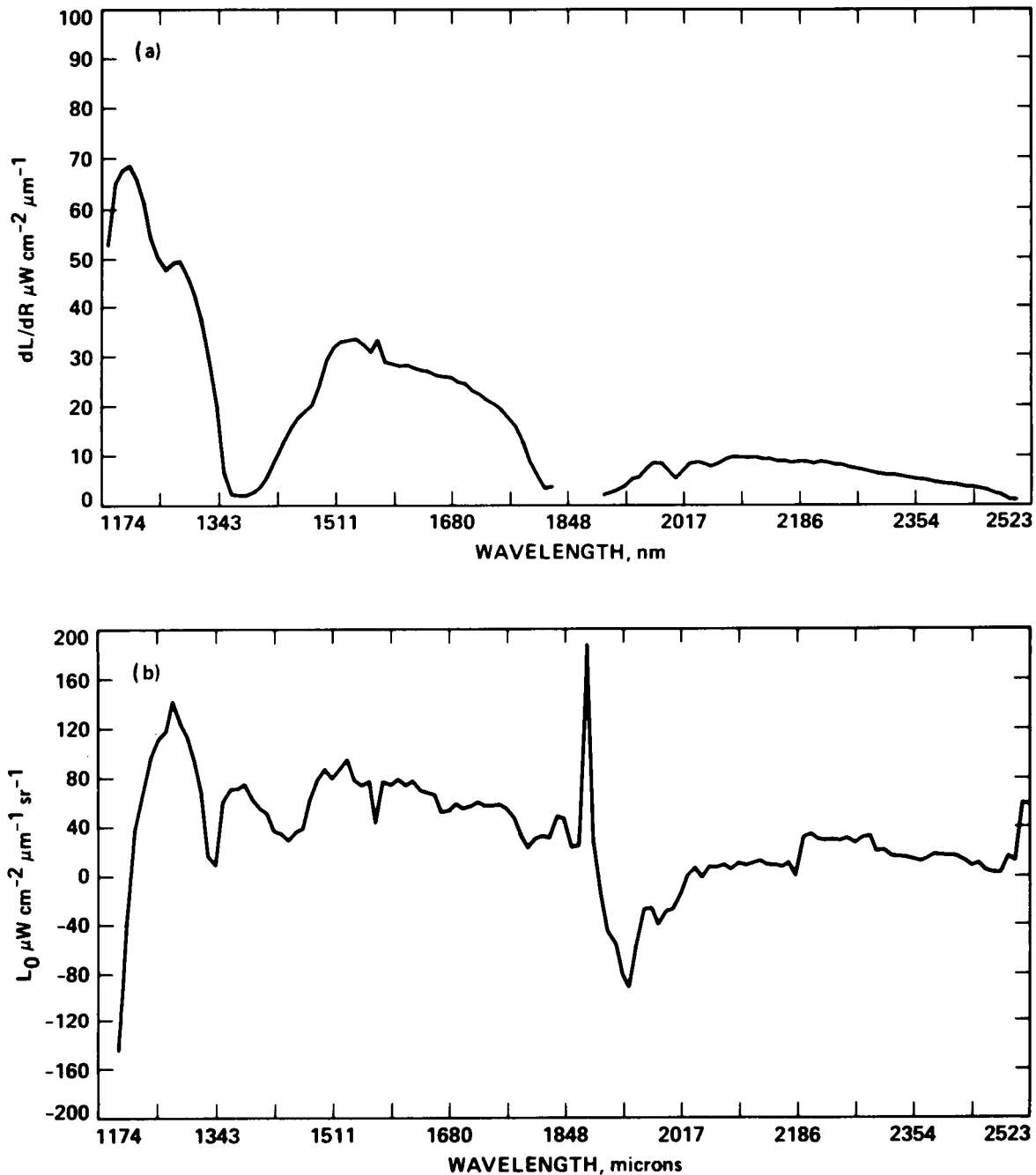
Figure 15. Values for the empirical calibration lines

field sampling of the dark target included both asphalt surface and bright lines painted on it, but no precise accounting of this mixture could be achieved because the runway is poorly resolved and the lines are not at all visible. If, for example, in the field-measured average spectrum the abundance of painted surface were overestimated, the slope of the resulting calibration line would be too steep. Accordingly, reflectances predicted for targets elsewhere would be too great. With respect to (2), the unknown, relatively bright target is surrounded on three sides by dark runways. If

41
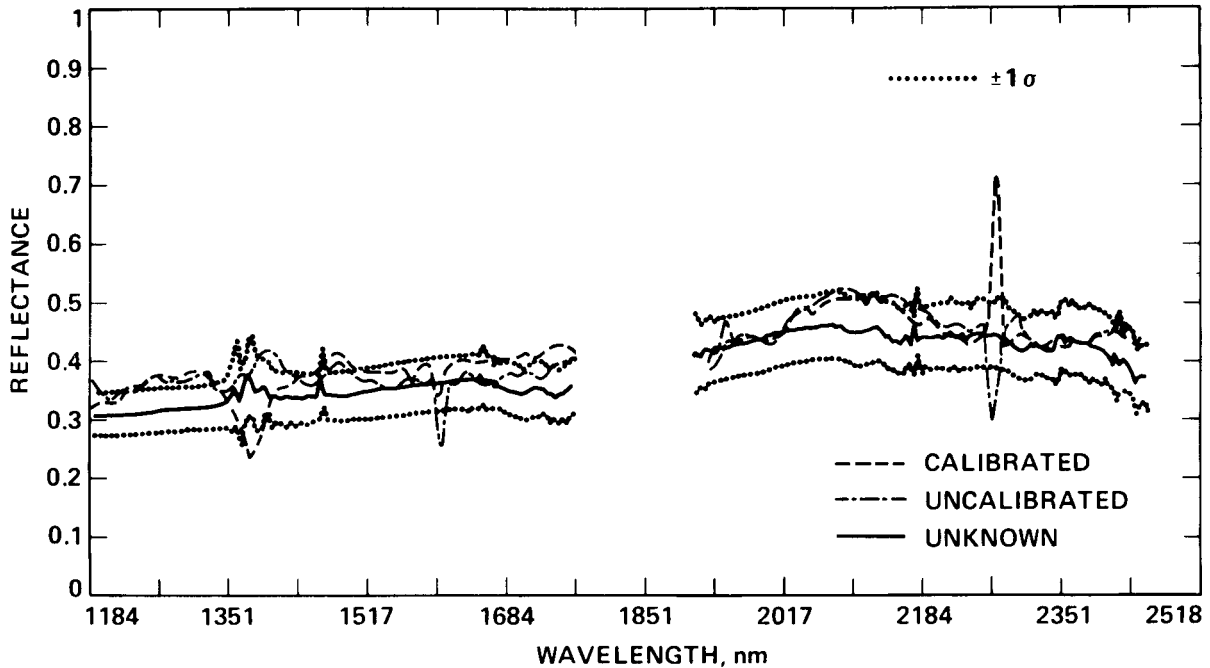
Figure 16. Comparison of spectra predicted for the unknown target from the empirical line method for both radiometrically reduced (calibrated) and unreduced (uncalibrated) data

this target is poorly resolved against the dark background, the apparent AIS response would be too low and would again lead to discrepancies of the sign observed.

Radiative Transfer Model

The radiative transfer modeling method of reduction to ground reflectance can be applied in a forward iterative fashion starting with the observed radiances and incrementally adjusting the surface reflectance value until the observed and predicted radiances equal each other. In order to apply this method, the following need to be supplied or estimated for the model: values of the optical depth for the atmosphere at each wavelength, the single scattering albedo, precipitable water abundance, concentration of CO_2, asymmetry factors for the aerosol scatterers, and variations of these quantities as height above the surface and horizontal position vary. As a first approximation, the LOWTRAN simulations and their comparisons with the observed radiances from AIS serve as a preliminary test of the ideas involved. LOWTRAN-6 supplies only a single scattering description of aerosol scattering (see Kneizys et al., 1983), so the use of it as a standard for comparison is less satisfactory at shorter wavelengths. For these problems the code developed by Diner and Martonchik (1984) will eventually be employed.

The principal source of concern here is the systematically lower value of the radiance returned from the laboratory calibration of AIS at each wavelength compared to the expected values from the LOWTRAN model. In a general way, if the laboratory calibration is taken as correct, then

directly adjusting the LOWTRAN model to match radiances leads to surface reflectances that are 30 to 50% too low compared to the field-determined numbers. The relationship is

$$R(AIS) = [L(AIS)/L(LOWTRAN)] \ R(PIDAS)$$

where R(AIS) is the surface reflectance implied by the AIS-observed radiance L(AIS), and R(PIDAS) is the surface reflectance as measured with PIDAS and used to produce a LOWTRAN model radiance L(LOWTRAN). Figure 8 shows L(AIS) and L(LOWTRAN), and Figure 17 is a plot of R(AIS) for the bright playa standard target. The appearance of uncompensated atmospheric bands in the predicted spectrum arises from dissimilarities between the assumed model and the observed spectrum in spectral resolution.

It does not seem worthwhile to go beyond this level of analysis, until the major extant discrepancies between the two data sets are removed.

SUMMARY

We have assembled a field experiment using AIS-2 over Rogers Lake, California to (1) provide an assessment of the engineering performance of the instrument with respect to in-flight radiometric calibration, spectral sampling interval, and signal-to-noise ratio and (2) compare various methods for the reduction of the data to ground reflectance, i.e., for atmospheric compensation. The Rogers Lake site presents a large, high-reflectance surface target (playa lake), dark targets (runways), and other surfaces (concrete runways) that can be used interchangeably as areas of known and unknown surface reflectance. Surface bidirectional spectral refléctance was determined with PIDAS. In addition, to support radiative transfer modeling and other exercises, we made observations of atmospheric optical depth, precipitable water abundance, and the ratio of direct to diffuse incident light.

With respect to the instrument-related questions we find (1) a spectral sampling interval between 20 and 30 as opposed to the ~10 nm expected from the instrument design, (2) a "signal-to-noise" ratio of 40 to 110, and (3) laboratory radiometric calibration radiances that are 30 to 50% lower than those expected.

In comparing the methods of data reduction we find the following: (1) The so-called scene average or log-residual method proves powerless to recover any feature of the surface reflectance, perhaps because of the homogeneity of the scene. (2) The empirical line method returns predicted surface reflectances that are within a few percent of the actual observed values using calibrated or uncalibrated data. The method encounters problems in detail in compensating for both water and CO_2 bands at various places in the spectrum. This suggests that both these gasses deserve detailed attention in the atmospheric modeling. (3) The radiative transfer question has been studied preliminarily using LOWTRAN-6. Apart from possible problems with the representation of scattering in this code, the
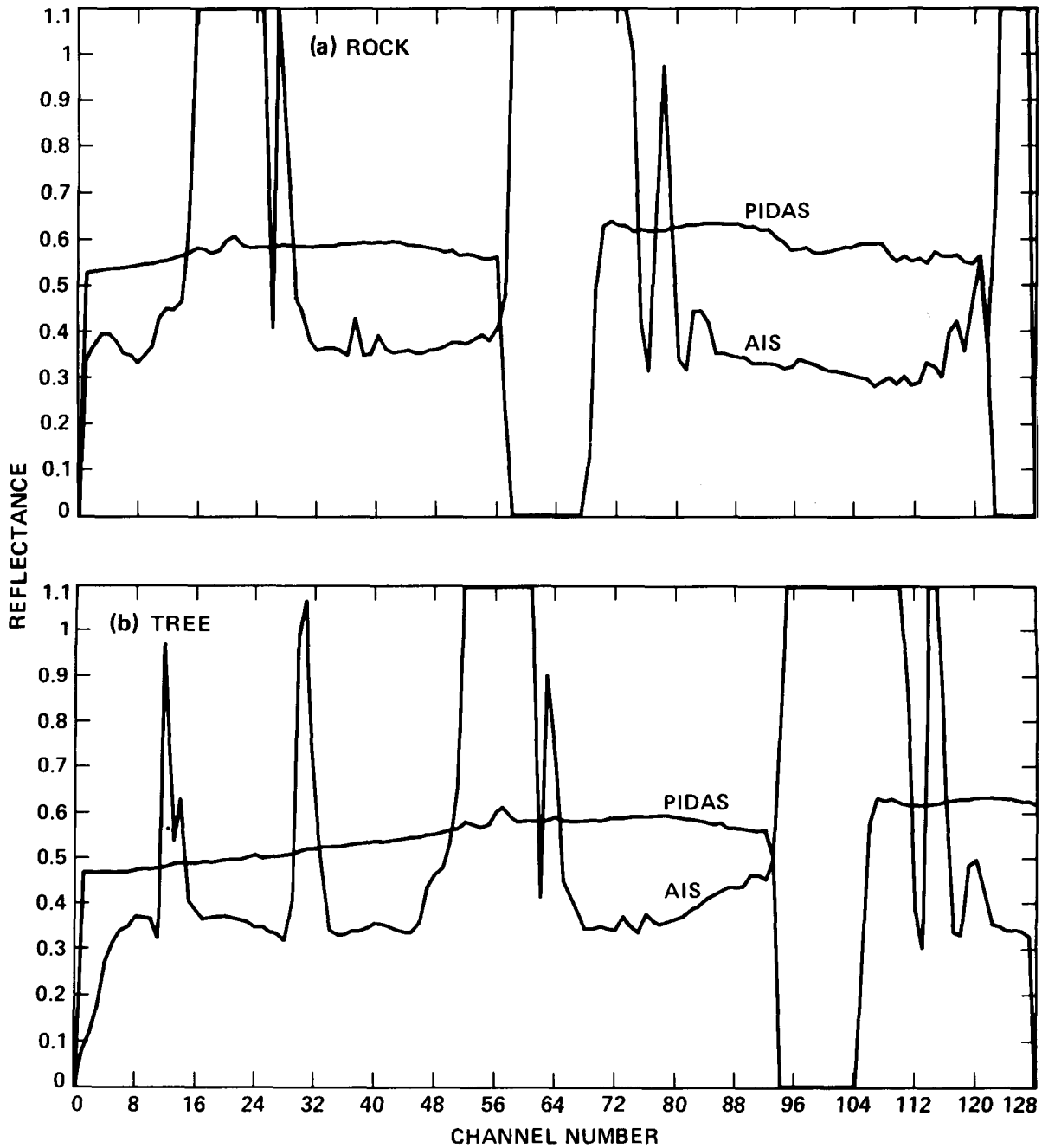
Figure 17. Surface reflectances derived from the AIS-2 data for the bright standard target using the LOWTRAN-6 atmospheric model: (a) rock mode and (b) tree mode

major concern for its application is the uncertain radiometry of AIS, since that code or any other relying on direct measurements of the radiance would return values of the surface reflectance lower than expected by 30 to 50% under solar illumination.

NOTE IN PROOF

An important factor in the radiometric analysis of AIS-2 presented earlier is the surface spectral reflectance returned by PIDAS, namely R(PIDAS). This quantity impacts directly the value of the expected radiance returned from LOWTRAN-6, as presented in Figure 8. P. Slater, R. Jackson and their associates (personal communication, 1987) have analysed surface reflectance measurements of the playa site taken with other radiometers in the field and have compared these data to measurements with a laboratory spectrometer. They find agreement between their laboratory and field-determined reflectances, which are 20 to 30% lower than the reflectance determined with PIDAS for the same site and time of observation. This difference, if true, reduces the radiance given by the LOWTRAN-6 simulation in Figure 8 by the same factor. The discrepancy between predicted and observed curves is accordingly narrowed and is roughly 30% of the AIS response itself rather than 60 or 70%. A similar reduction in the differences between the observed and calculated spectra of the test area shown in Figure 17 is also achieved if the reflectance determinations of Slater et al. are used.

ACKNOWLEDGEMENTS

REFERENCES

Airborne Imaging Spectrometer Supplement. Supplement to the Science Investigators' Guide to AIS Data. May 1, 1986. JPL internal document, Jet Propulsion Laboratory, Pasadena, CA, 20 pp.

Cocks, T.D., and A.A. Green. 1986. Airborne spectroradiometry: The application of AIS data to detecting subtle mineral absorption features. Proceedings of the Second Airborne Imaging Spectrometer Data Analysis Workshop (G. Vane and A. F. H. Goetz, eds.). JPL Publication 86-35, Jet Propulsion Laboratory, Pasadena, CA, pp. 52-62.

Conel, J.E., S. Adams, R.E. Alley, G. Hoover, and S. Schultz. 1986. Analysis of AIS radiometry with emphasis on determination of atmospheric properties and surface reflectance. Proceedings of the Second Airborne Imaging Spectrometer Data Analysis Workshop (G. Vane and A. F. H. Goetz, eds.). JPL Publication 86-35, Jet Propulsion Laboratory, Pasadena, CA, pp. 31-51.

Conel, J.E., R.O. Green, G. Vane, C.J. Bruegge, R.E. Alley, and B.J.
    Curtiss. 1987a. Airborne Imaging Spectrometer-2: Radiometric and
    spectral characteristics and comparison of ways to compensate for the
    atmosphere. Paper presented at SPIE 1987 Symposium, San Diego, CA,
    August 1987.

Conel, J.E., S. Adams, R.E. Alley, G. Hoover and S. Schultz. 1987b. AIS
    radiometry and the problem of contamination from mixed spectral
    orders. Remote Sensing of Environ. Elsevier (in press).

Diner, D.J., and J.V. Martonchik. 1984. Atmospheric transfer of radiation
    above an inhomogeneous non-Lambertian reflective ground-I. Theory. J.
    Quant. Spectrosc. Radiat. Transfer. 31 (2): 97-125.

Goetz, Alexander F.H. 1987. The Portable Instant Display and Analysis
    Spectrometer (PIDAS). In Proceedings of the 3rd Airborne Imaging
    Spectrometer (AIS) Data Analysis Workshop (G. Vane, ed.). JPL
    Publication 87-30, Jet Propulsion Laboratory, Pasadena, CA.

Green, A.A., and M.D. Craig. 1985. Analysis of aircraft spectrometer data
    with logarithmic residuals. Proceedings of the Airborne Imaging
    Spectrometer Data Analysis Workshop, JPL Publication 85-41, Jet
    Propulsion Laboratory, Pasadena, CA, pp. 111-119.

Hansen, J.E., and L.D. Travis. 1974. Light scattering on planetary
    atmospheres. Space Science Reviews. 16: 527-610.

Kneizys, F.X., E.P. Shettle, W.O. Gallery, J.H. Chetwynd, Jr., L.W. Abrew,
    J.E.A. Selby, S.A. Clough, and R.W. Fenn. 1983. Atmospheric
    Transmittance/Radiance: Computer code LOWTRAN 6. AFGL-TR-83-0187,
    AFGL Hanscom AFB, MA. 200 pp.

LaRocca, A.J. 1978. Atmospheric absorption, Chap. 5, in The Infrared
    Handbook (W.L. Wolfe and G.J. Zissis, eds.). Environmental Research
    Institute of Michigan, Ann Arbor, MI, pp. 5-3 - 5-132.

Roberts, D.A., Y. Yamaguchi, and R.J.P. Lyon. 1986. Comparison of various
    techniques for calibration of AIS data. Proceedings of the Second
    Airborne Imaging Spectrometer Data Analysis Workshop (G. Vane and
    A.F.H. Goetz, eds.). JPL Publication 86-35, Jet Propulsion Laboratory,
    Pasadena, CA, pp. 21-30.

Solomon, J.E. 1984. Thoughts on atmospheric "corrections" for AIS imagery.
    JPL IOM IAS: 384-84-JES102ed. JPL internal document, Jet Propulsion
    Laboratory, Pasadena, CA.

SPAM Handbook. 1987. Spectral Analysis Manager, Software for imaging
    spectrometry data analysis, October 1, 1986. JPL internal document,
    Jet Propulsion Laboratory, Pasadena, CA.

Tucker, D. 1987. Integrating sphere calibration - bulb set #2. JPL
    internal document, Jet Propulsion Laboratory, Pasadena, CA.

Vane, G. 1986. Introduction to the Proceedings of the Second Airborne
    Imaging Spectrometer (AIS) Data Analysis Workshop. In <u>Proceedings of
    the Second Airborne Imaging Spectrometer (AIS) Data Analysis Workshop</u>
    (G. Vane, and A.F.H. Goetz, eds.). JPL Publication Number 86-35, Jet
    Propulsion Laboratory, Pasadena, CA, pp. 1-16.